Applied Acoustics, Volume 70, Issue 4, April 2009, Pages 547–555

Seeded fault detection on helical gears with Acoustic Emission

Babak Eftekharnejad, D. Mba
School of Engineering, Cranfield University, Bedford, MK43 0AL, England
Email: b.eftekharnejad@cranfield.ac.uk

Abstract

Acoustic Emission (AE) is one of many technologies for health monitoring and diagnosis of rotating machines such as gearboxes. Although significant research has been undertaken in understanding the potential of AE in monitoring gearboxes this has been solely applied to spur gears. This report presents an experimental investigation that assesses the effectiveness of AE in identifying seeded defects on helical gears; the first known attempt. In addition, a comparison between vibration and AE in identifying the presence of defects is presented. It was concluded that AE offered more sensitivity than vibration analysis for the defect identification on helical gears.

1 Introduction

Acoustic Emission (AE) is defined as the range of phenomena that results in the generation of structure-borne and fluid-borne (liquid, gas) propagating waves due to the rapid release of energy from localised sources within and/or on the surface of a material [1]. The application of the acoustic emission technology in research and industry is well-documented [2]. In relation to gearboxes a few investigators have assessed the application of AE technology for diagnostic and prognostic purposes [3-6]. Others [7-10] applied AE in detecting bending fatigue on spur gears and noted that AE is more sensitive to crack propagation than vibration and stiffness measurements. Again, AE was found to be more sensitive to the scale of surface damage than vibration analysis.

Toutountzakis et al [11] employed a back-to-back test rig to investigate the effectiveness of AE in identifying seeded defects on spur gears. It was concluded that defect detection with AE is fraught with difficulties and recommended further experiments to achieve better understanding on the influence of operational variables on the generation of AE. Toutountzakis,T. et. al [12], Raja Hamzah, R.I. et. al [13],

and Tan,Chee Keong et. al [14, 15] investigated the influence of operational factors such as speed, torque and specific film thickness on the generation of Acoustic Emission on spur gears. Asperity contact was noted to be a significant source of AE under Elastohydrodynamic lubrication regime, which is synonymous with gears [14].

To date, there has been no attempt to understanding the mechanisms for generating AE activity in helical gears, nor has an attempt to assess the ability of AE to identify defects in such gears; considering helical gears are a major component of gearbox applications worldwide this is rather surprising. It is also known that the meshing mechanisms for a helical gear is progressive due to the gradual increase and decrease in contact length over a particular tooth whilst the spur gear mesh has a constant contact length throughout the gear mesh. This report presents an experimental investigation that assesses the effectiveness of AE monitoring techniques for identification of seeded defects on helical gears. In addition, the effect of gradual defect growth is explored.

2 EXPERIMENTAL SETUP

2.1 Test-rig

The gearbox test rig employed was of back-to-back arrangement (see fig 1), powered by 1.1KW motor with helical (214M15) steel test gears, see table 1. The gearbox was lubricated with Mobile gear 636 oil, see table 2, and operated at a speed of 690rpm.

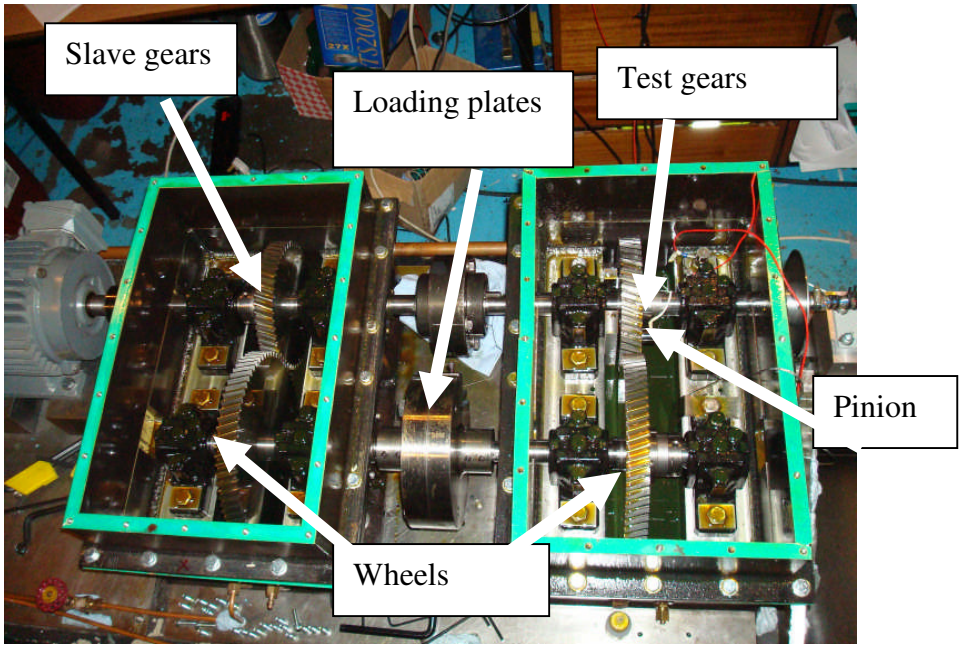

Figure 1 Gearbox test rig

Table 1 Specification of test gears

	Pinion	Wheel
Number of teeth	51	70
Module	3 mm	3 mm
Pressure angle	20º	20º
Helix angle	17.5º	17.5º
Contact ratio	1.7	1.7
Face width	25.1 mm	25.1 mm
Direction	Right Hand	Left Hand
Hardness	137 Hv30	137 Hv30
Surface roughness	1.327 µm	1.327 µm
Pitch circle diameter	160.65 mm	220.50 mm
Size of Addendum	3 mm	3 mm
Size of Dedendum	3.75 mm	3.75 mm

Table 2 Specification of the oil

Lubricant properties	Mobile Gear 636
Kinematics viscosity@40º	664 (cSt)
Kinematics viscosity@100º	62.8(cSt)
Viscosity index ASTM D2270	165
Density @ 15º ASTM D4052	0.87

2.2 Instrumentation

A wide-band AE sensor (type WD, from Physical Acoustic Limited) was employed to measure AE throughout the test. The AE sensor was fixed on the pinion using super glue (see figure 2). The AE sensor was of differential type with a relative flat response of between 100 kHz to 1 MHz.

The cable from the AE sensor was fed through a narrow longitudinal duct inside the input shaft and connected to the slip ring. The slip ring (PH-12, IDM Electronic Ltd) placed at the end of test gearbox. AE was recorded with MISTRAS AE DSP-32/16 data acquisition card at a sampling rate of 10 MHz. An accelerometer (ISOBASE 236 Endevco) with operating range of between 10 and 8000Hz was mounted on the bearing pedestal inside the test gearbox (see figure 2). A charge amplifier (Endevco 2721B) was employed with a PersonalDaq3000 external acquisition board. All vibration data was recorded at a sampling rate of 10 KHz. In order to observe temperature during the experiment a J-type thermocouple, rated from -60 to +850ºC, was also placed inside the oil bath.

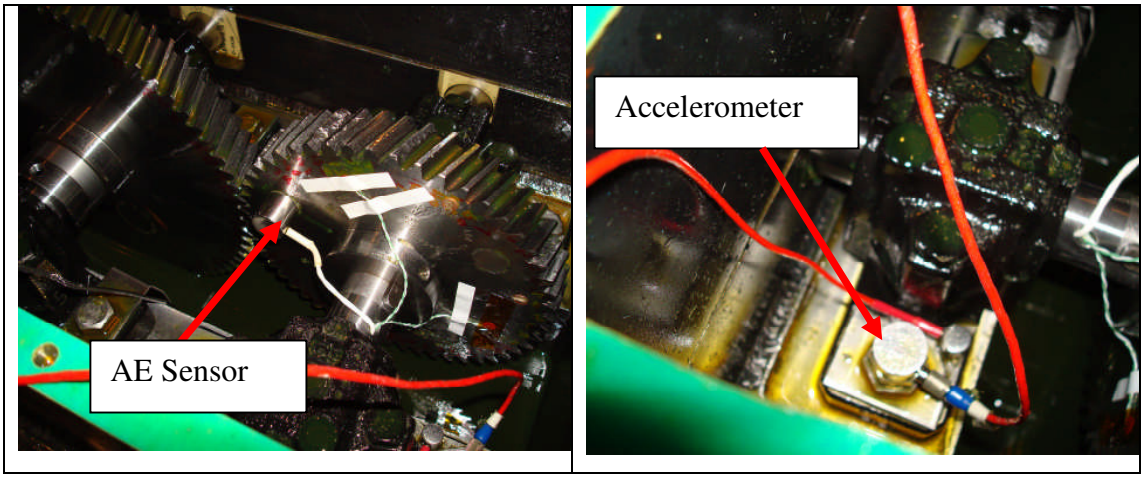

Figure 2 AE sensor placement **Accelerometer position on bearing**

As this experiment centred on assessing the applicability of AE for identifying seeded defects on helical gears, it was paramount that any data recorded was taken from a defined circumferential point every revolution. For this reason, an optical triggering mechanism was employed. The triggering system consisted of metal disk with 2mm diameter hole and an optical sensor. Each time the hole passed trough the optical sensor the AE and vibration acquisition systems were triggered (see figure 3).

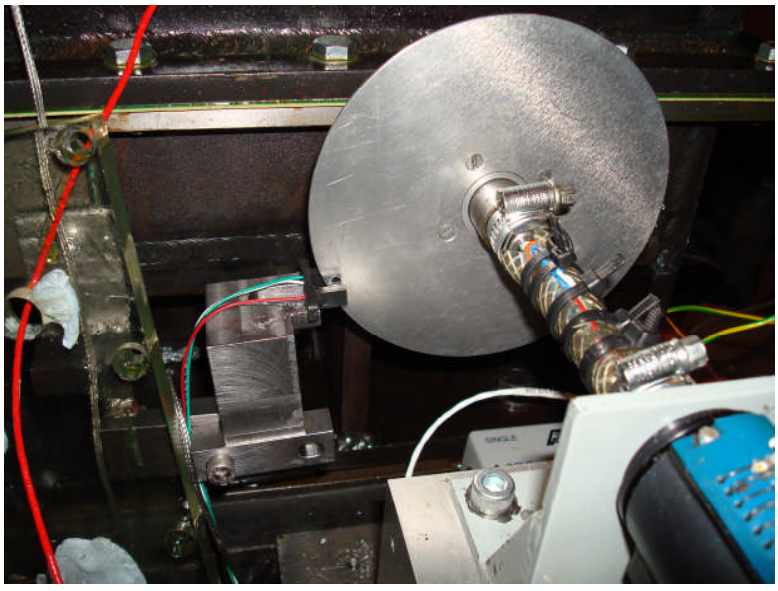

Figure 3 Data acquisition triggering mechanism

3 Test procedure

Prior to the testing the gearbox was run for 3-hours at 380Nm so as to allow the gearbox to dynamically settle and reach a stabilized temperature; in this instance 60ºC. It was essentail to capture AE and vibration data that included the defective tooth and as such and acquisition time frame, or window, of 16-teeth was set whereby the trigger mechanism ensured an acquisition duration of 0.0256-seconds, corresponding to 16 teeth at 690 rpm. To begin the tests a defect free recording of AE and vibration was undertaken. The gearbox was then stopped and the torque set to 250Nm and run for 5-minutes to accommodate the new dynamic condition. Again, defect free AE and vibration data were captured for the same acquisition window. The same procedure was repeated at 180Nm. The defect free condition will be referred to defect-0, see table 3.

In order to carry out the seeded defect test, the test rig was stopped and the first defect (defect-1, see table 3) introduced on the seventh tooth using a drill (see figure 4). The gearbox was then started and vibration and AE data for the time frame encompassing the damaged tooth was acquired instantly. The significance of the instantaneous recording was to allow the authors to explore the influence of surface/material deformation on the levels of AE and vibration as some investigators had suggested [11, 16]. The gearbox was allowed to operate until the temperature reached 60ºC after which AE and vibration signals were again recorded for the specific defect condition. The same procedure was repeated at 250Nm and 180Nm respectively. The test sequence continued for six more defects conditions as detailed in table 3. Eventually, four sets of data for each defect were produced. The first was associated with data at 380 Nm torque, captured immediately after the defects were generated, and referred as ‘D’ throughout this report. Other sets of data corresponded to the data at 380Nm, 250Nm and 180Nm for constant temperature (60 ° C) and labelled as ‘A’, ‘B’ and ‘C’ respectively.

Twenty sets of AE data were recorded for every defect and load condition. Each AE data file corresponded to a waveform representing 16 teeth with time length of 0.0256 seconds (see figure 5). Similarly, vibration data was captured at 10kHz sampling rate over a time window of 0.0256sec. The vibration data was averaged

Table 3 Details of seeded defects

Defect type	Size(mm^2)	Depth(mm)	Removed Volume(mm^3)	Defect tooth
Defect-0	0	0	0	7
Defect-1	18.88	0.1	1.888	7
Defect-2	28.71	0.2	5.742	7
Defect-3	41.22	0.5	20.61	7
Defect-4	17.5	1	17.5	7
Defect-5	15	0.8	12	7
Defect-6	158.75	0.2	31.75	11
Defect-7	163.5	0.2	32.7	15

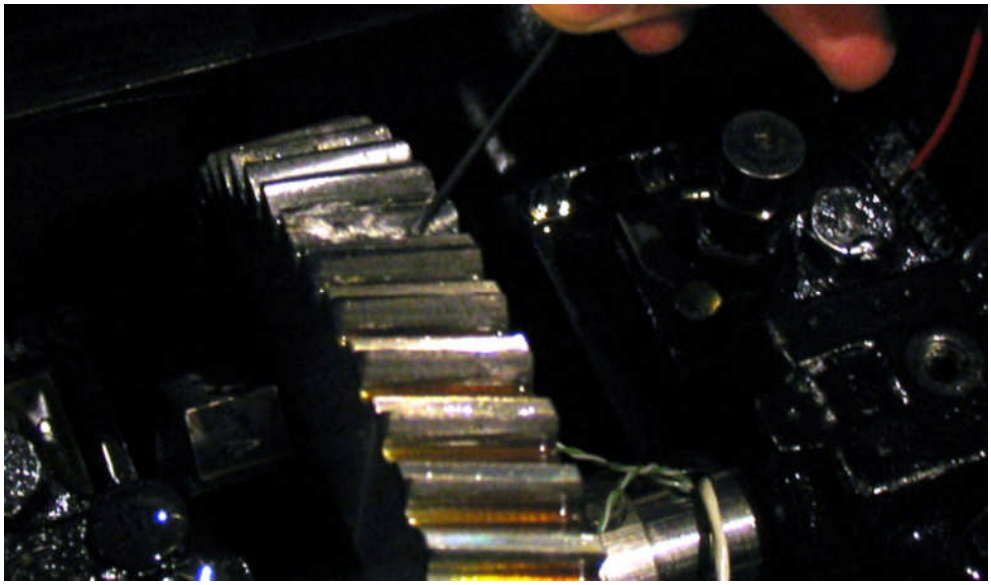

Figure 4 Seeded defect on the tooth

4 Result and discussion

4.1 Results based on Acoustic Emission monitoring

A typical waveform associated with the defect free condition at 380Nm is presented in figure 5. Continuous type AE waveform is dominant although there also existed transient AE bursts whose amplitude exceeds the underlying continuous wave; the frequency of the periodicity of the AE bursts represented the number of meshing teeth within the acquisition window. This is similar to observations of AE waveforms in spur gear mesh in which both continuous and transient type forms of AE activity were apparent [14]. Tan et al [14] concluded that rolling contact on the pitch line of the

spur gear mesh was responsible for generating of high amplitude AE transient burst, whilst sliding contact was attributed to the generation a large portion of the continuous waveform.

In relation to helical gears, contact between a specific gear pair begins as a minute contact point which increases in contact length on the engaging pair whilst decreasing in contact length on the disengaging pair of gears. As such, the contact length varies along the pitch line of the helical gears whereas in spur gears the contact length remains constant. In addition, the continued variation in the contact length during meshing of helical gears [17], which directly influences the load conditions experienced by the gear, will lead to instantaneous changes in oil film thickness. Therefore, AE waveforms associated with the helical gear mesh were expected to be of the continuous type with amplitude variations attributed to the gear mesh, see figure 5.

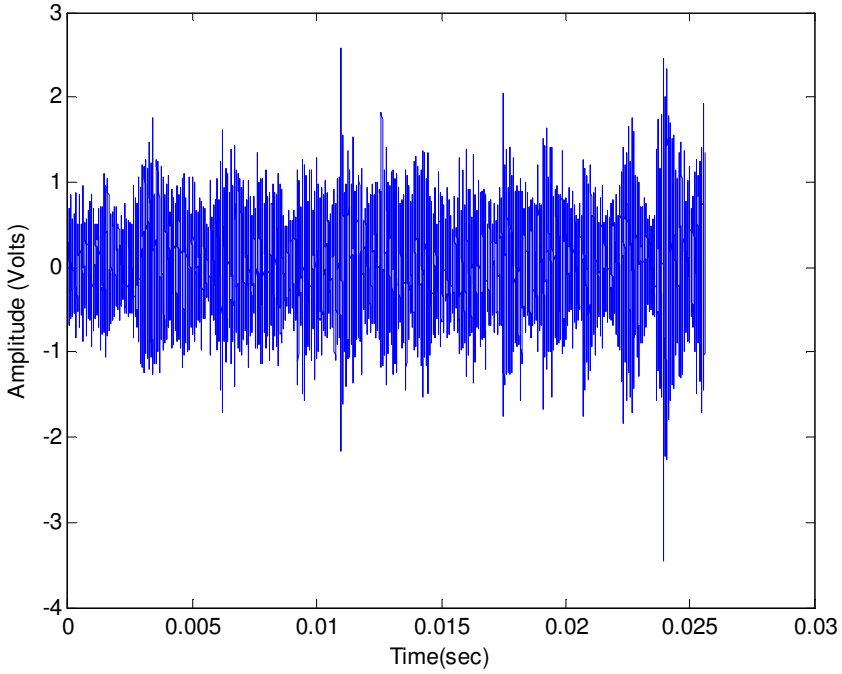

Figure 5 Mixed modes AE waveform associated with a defect free condition

Figure 6 shows typical AE waveforms associated with each defect condition which showed relatively large transient AE bursts over continuous operational AE levels. The transient AE bursts where noted to occur at the exact tooth where the defect was

seeded, see figure 6. Such observations were not noted in a similar test with spur gears, i.e., the seeded defects were not evident in the waveforms [11, 16].

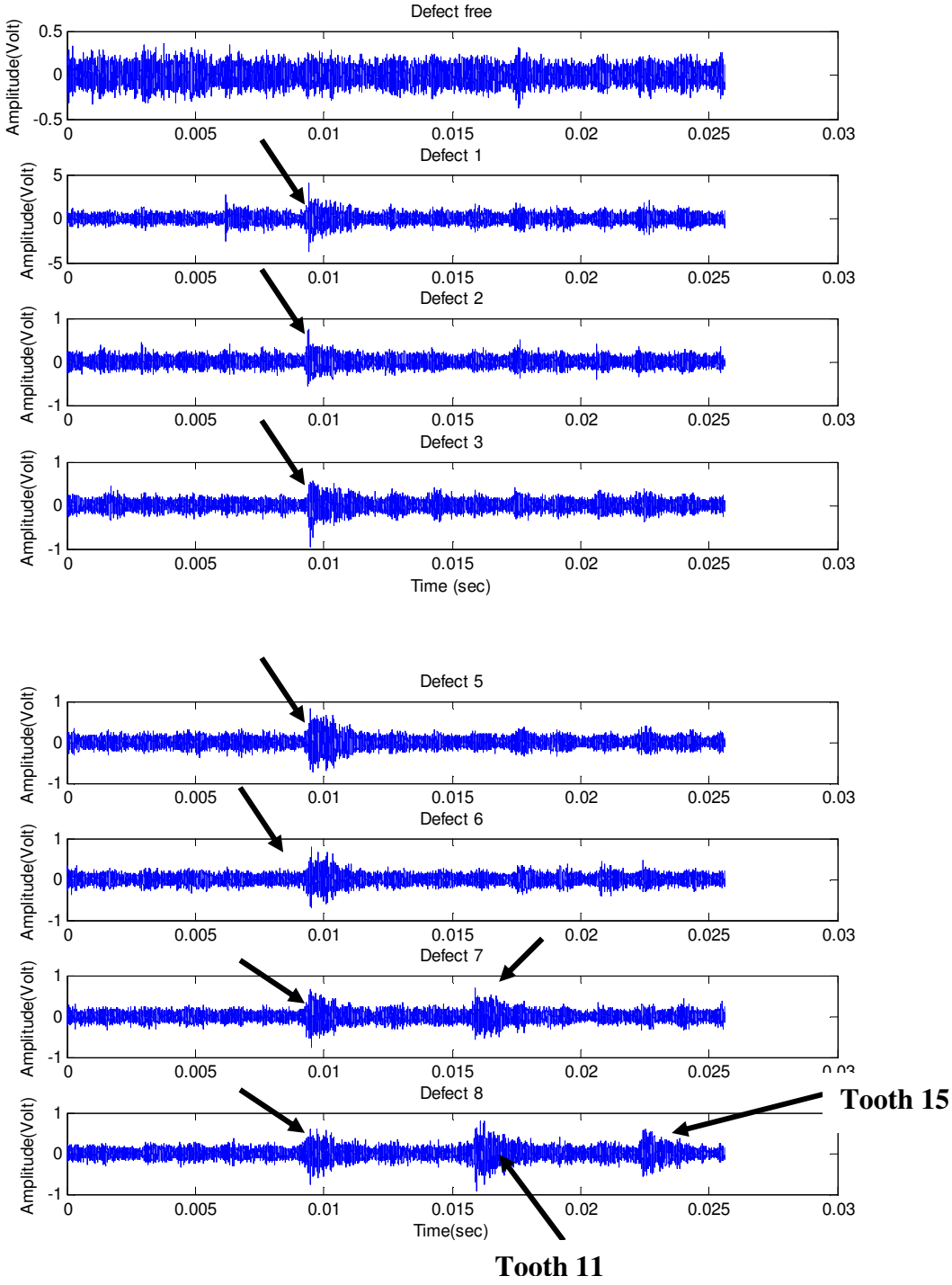

Figure 6 **Waveforms associated with each defect for 'A' condition**

AE r.m.s values for all test conditions were obtained by averaging all r.m.s values associated with all twenty data files per fault and load condition, see figure 7, and,

figure A1 and table A1 in the Appendix. In general an increase in AE r.m.s levels for increasing defect size for all test load conditions was noted, see figure 7. For load conditions B (250Nm) and C (180Nm) an increase in AE r.m.s levels with increasing defect width and number of defective teeth was evident though for test condition A (380Nm) and D (380Nm) a similar trend was observed between 'defect-free' and defect-3 conditions after which r.m.s values decreased slightly from defect-3 to defect-5; AE r.m.s levels increased again from defect-5 to defect-7. The exact reason for this observation is addressed later in the paper. It was noted that the increased load condition did not necessarily always imply increased AE levels. This was noted for load condition 'A' (380Nm) after defect-4. The exact reason for this decrease is still unclear.

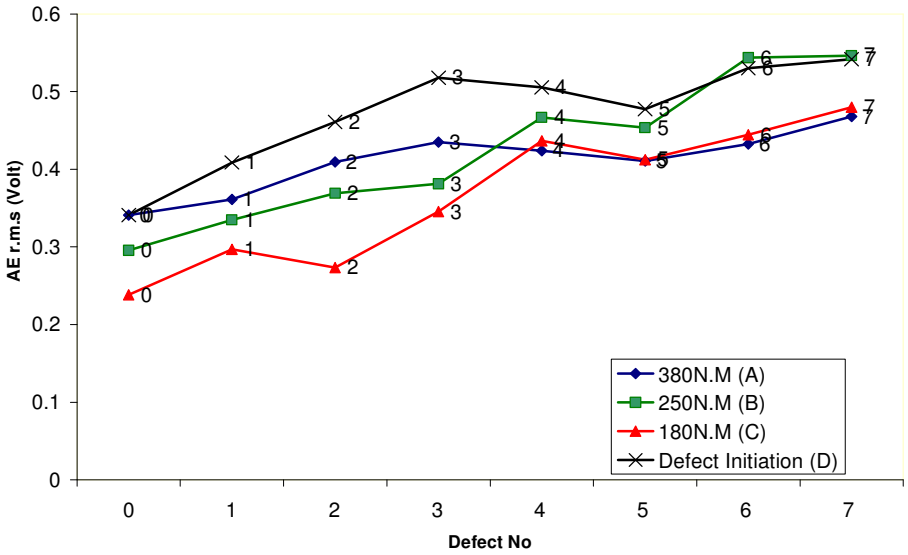

Figure 7 AE r.m.s values for each defect condition

Of interest is that the AE r.m.s levels of the initial defect condition (D) were relatively higher than all other test conditions but for one test condition (Defect-6, 250Nm). This was not surprising giving that asperity contact has been shown to be a major source of AE generation during gear mesh [14, 18, 19]. Also, as noted by others [11, 16, 21] the influence of material protrusions around the edge of a seeded defect cavity which are relatively higher than the rest of the gear surface roughness, caused as a direct result of generating seeded faults, will generate AE activity. Giving that after several thousand of revolutions (1,300,000) the protrusions will be progressively

flattened resulting in a relative reduction in AE levels as noted in figure 7; this confirms the postulations of Tan et al [16] and Al-Dossary et. al [21]. Figure 8 schematically presents the process of AE generation due to the presence of protrusions.

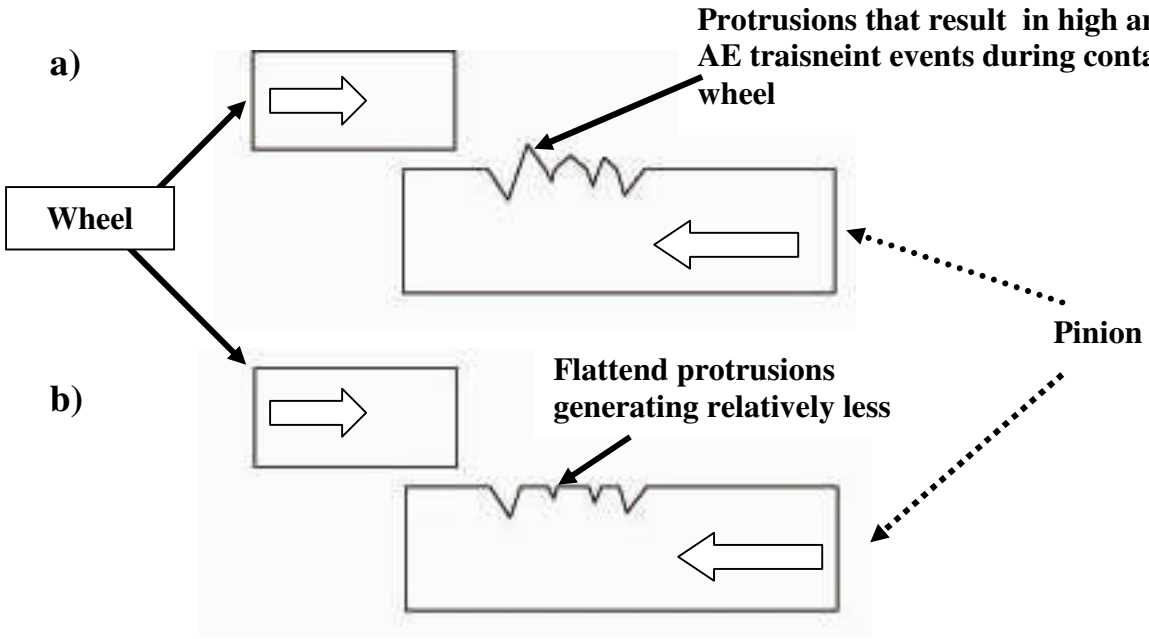

Figure 8 Schmatic of the effect of protrusions on AE activity

To address the reason for the decrease in AE levels with increasing defect size, as noted for test conditions A and D (defect-3 and defect-5), the approximate volume of each defect was calculated following casting of the defect onto 'plaster' so as to obtain a three-dimensional profile. Plotting the volume removed against AE r.m.s yielded an interesting observation, see figure 9. A direct relationship between the defect volume and AE was noted for test conditions 'A' and 'D'; in some cases where the defect width was relatively wide but the volume removed relatively less (e.g., defect-5 was wider than defect-3 but the volume removed in defect-3 was more than defect-5), the AE r.m.s levels were higher for the case of the larger volume removed. For cases B and C the observation was not similar, particularly at defect-3. This has some implications particularly in understanding other influencing sources of AE during meshing. This suggested the influence of the mechanism of interaction of the fluid within the defect cavity would appear to offer a source of AE activity. This particular observation was investiagetd further. To this end further tests were

undertaken. A gear tooth was selected and holes of varying depth (volume) and a fixed diameter (2.5mm) were drilled into the tooth, see table 4 and figure 10.

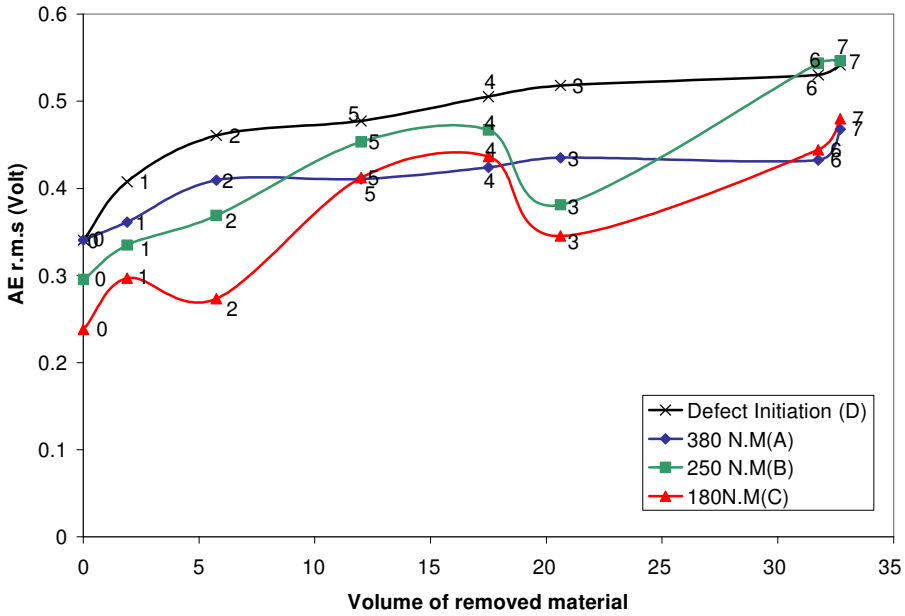

Figure 9 AE r.m.s against volume of removed material for all condition

Table 4 Specification of increasing defects volume on a fixed tooth at 380Nm

Defect No	Depth
0	Defect free
1	1mm
2	3mm
3	5mm
4	7mm
5 (Second hole)	7mm
6 (Third hole)	7mm

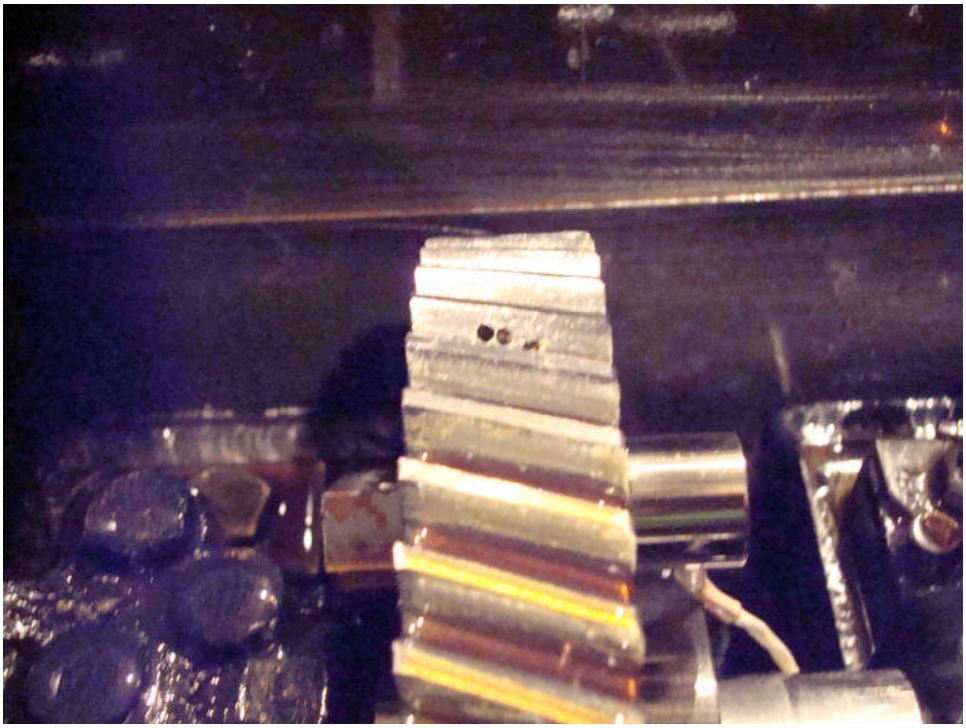

Figure 10 Drilled holes on the tooth surface

After each depth was seeded the rig was operated for 45minutes (3,000,000 revolutions) before any AE data was recored. This was to ensure the temparture remianed contanst throughout the tests. Results, presented in figure 11, showed that an increase in AE r.m.s was a direct consequence of increased cavity volume, strongly supporting the notion that the entrapped lubricant within a cavity (pit, spall, etc) will also contirbute to the level of AE measured. The sampling rate applied for these poarticular tests was 4MHz and a total of 65,536 data points were recorded per file, of which over 25-data files were acquired for each volume condition. This is the first known attempt at investigating this phenomonon and will, in the fullness of time, lead to future investigations. A typical waveform associated with these volumetric tests is presented in figure 12 and it shows that the holes did not cause any materal producions nor did they result in an AE waveform typical of the presence of a defect as seen in figure 6.

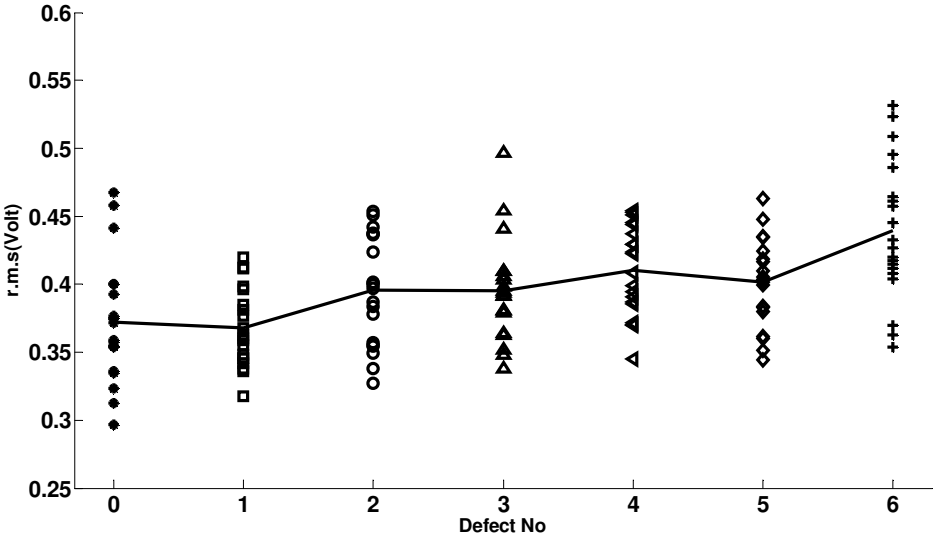

Figure 9 AE r.m.s level against depth of the drilled hole

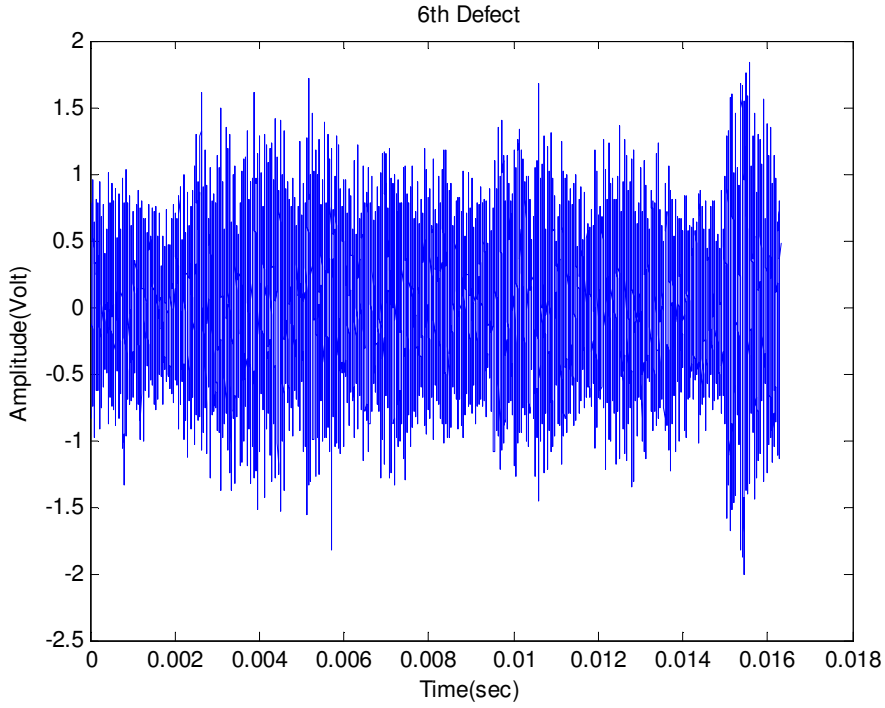

Figure 12 Typical waveform for volumetric defect

4.2 Results based on vibration signatures

Twenty sets of data for each defect at different conditions based on 10 KHz sampling rate were captured and synchronously averaged. Each data set acquired was associated with a time window encompassing 16 teeth.

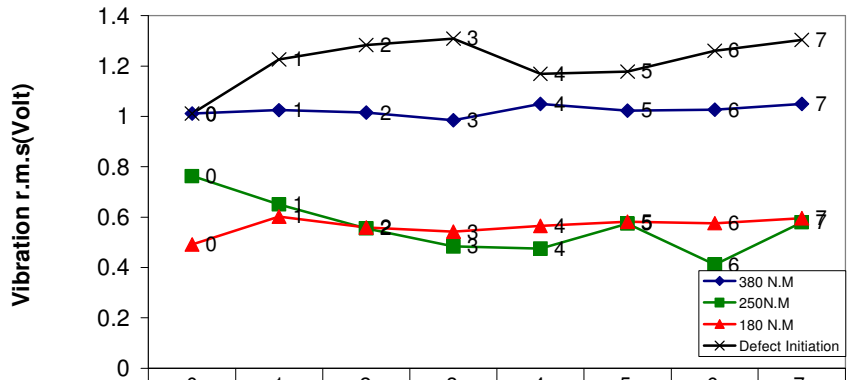

	0	1	2	3	4	5	6	7
380 N.M	1.0118	1.0249	1.0147	0.9848	1.049	1.0234	1.0263	1.0496
250N.M	0.7629	0.651	0.5561	0.4839	0.4743	0.5747	0.4115	0.5798
180 N.M	0.4923	0.6027	0.5593	0.5428	0.565	0.5815	0.5758	0.5954
Defect Initiation	1.0118	1.2265	1.2839	1.3087	1.1691	1.1779	1.2608	1.3036

Defect No

Figu re 103 Vibration RMS level for each defect at different loading condition

Vibration r.m.s values for each test condition are illustrated in figure 13. The vibration r.m.s level at D-condition was relatively higher than for all other conditions for the reasons discussed earlier. In addition, the plastic deformation of protrusions around the defect will lead to alteration in stiffness and consequently growth in vibration [20]. In comparison to AE r.m.s levels, the vibration r.m.s levels remained relatively constant irrespective of defect condition reiterating the widely held view that AE is relatively more sensitive than vibration [2], see figure 13.

Figure 14 illustrates the vibration energy values for each defect condition calculated by integrating the frequency spectrum of the signal condition over the frequency range encompassing meshing frequency and its side bands and harmonics of the side bands (350 to 850 Hz). It was noted as the defect extended along the face width an increase in energy value was noted at ‘D’ and ‘A’ conditions but vibration energy levels remained constant at test conditions ‘B’ and ‘C’. Furthermore, it was noticed that as the torque level reduced energy value associated with each defect decreased.

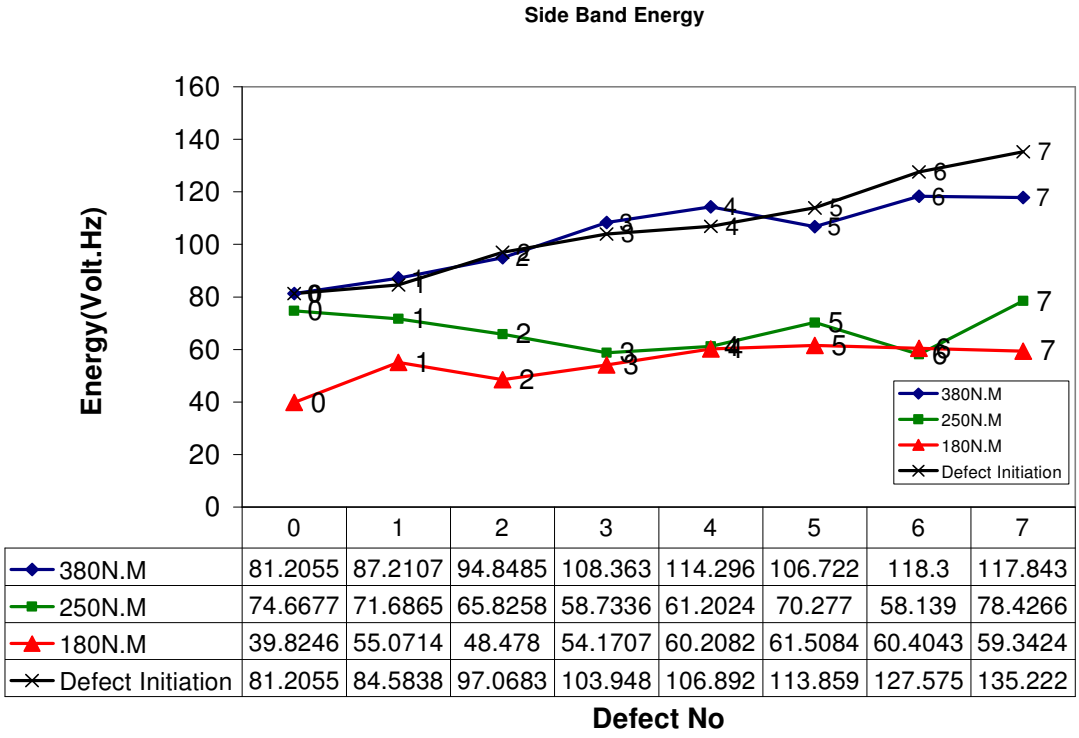

	0	1	2	3	4	5	6	7
380N.M	81.2055	87.2107	94.8485	108.363	114.296	106.722	118.3	117.843
250N.M	74.6677	71.6865	65.8258	58.7336	61.2024	70.277	58.139	78.4266
180N.M	39.8246	55.0714	48.478	54.1707	60.2082	61.5084	60.4043	59.3424
Defect Initiation	81.2055	84.5838	97.0683	103.948	106.892	113.859	127.575	135.222

Figure 114 Energy values for sidebands around gear meshing frequency

5 Conclusion

The following conclusions are made based on observation during the experiment.

1. Seeded defects in helical gears are evident in the AE waveform. This not the case for spur gears.
2. There is a direct relation between volume of removed material and AE r.m.s; this is the first observation of its kind and will be subject to future investigation.
3. Measurement AE r.m.s levels have been shown to be more sensitive to identification of seeded defects on helical gears than vibration analysis.

6 References

[1] ISO 22096, 2007, "Condition Monitoring and Diagnostics of Machines. Acoustic Emission," .

[2] Mba, D., and Rao, R. B. K. N., 2006, "Development of Acoustic Emission Technology for Condition Monitoring and Diagnosis of Rotating Machines: Bearings, Pumps, Gearboxes, Engines, and Rotating Structures," Shock and Vibration Digest, **38**(1) pp. 3-16.

[3] Wheitner, J., Houser, D., and Blazakis, C., 1993, "Gear tooth bending fatigue crack detection by acoustic emission and tooth compliance," ASME, 93FTM9, .

[4] Singh, A., Houser, D. R., and Vijayakar, S., 1999, "Detecting Gear Tooth Breakage using Acoustic Emission: A Feasibility and Sensor Placement Study," Journal of Mechanical Design, Transactions of the ASME, **121**(4) pp. 587-593.

[5] Miyachika K., Oda S., and Koide T., 1995, "Acoustic Emission of Bending Fatigue Process of Spur Gear Teeth," Journal of Acoustic Emission, **13**(1/2) pp. S47-S53.

[6] Miyachika K., Zheng, Y., Tsubokura, K., 2002, "Acoustic Emission of bending fatigue process of supercarburized spur gear teeth," Progress in Acoustic Emission *XI*, Anonymous The Japanese Society for NDI, pp. 304-310.

[7] E.Siores, and E.Negro, 1997, "Condition Monitoring of Gear Box using Acoustic Emission Testing," Material Evaluation, **55**(2) pp. 183-184,185,186,187.

[8] H. Sentoku, 1998, "AE in Tooth Surface Failure Process of Spur Gears," Journal of Acoustic Emission 16, **1-4**pp. S19-S24.

[9] Tandon.N, and Mata.S, 1999, "Detection of Defects in Gears by Acoustic Emission Measurements," Journal of Acoustic Emission, **17**(1-2) pp. 23-24,25,26,27.

[10] Amani RAAD, Fan ZHANG, Bob RANDALL, 2003, "On the comparison of the use of AE and vibration analysis for early gear fault detection," The Eight Western Pacific Acoustics Conference, Anonymous .

[11] Toutountzakis, T., Tan, C. K., and Mba, D., 2005, "Application of Acoustic Emission to Seeded Gear Fault Detection," NDT and E International, **38**(1) pp. 27-36.

[12] Toutountzakis, T., and Mba, D., 2003, "Observations of Acoustic Emission Activity during Gear Defect Diagnosis," NDT&E International, **36**(7) pp. 471-7.

[13] Raja Hamzah, R. I., and Mba, D., 2007, "Acoustic Emission and Specific Film Thickness for Operating Spur Gears," Journal of Tribology, **129**(4) pp. 860-867.

[14] Tan, C. K., and Mba, D., 2006, "A Correlation between Acoustic Emission and Asperity Contact of Spur Gears Under Partial Elastohydrodynamic Lubrication," International Journal of COMADEM, **9**(1) pp. 9-14.

[15] Tan, C. K., Irving, P., and Mba, D., 2007, "A Comparative Experimental Study on the Diagnostic and Prognostic Capabilities of Acoustics Emission, Vibration and Spectrometric Oil Analysis for Spur Gears," Mechanical Systems and Signal Processing, **21**(1) pp. 208-233.

[16] Tan, C. K., and Mba, D., 2005, "Limitation of Acoustic Emission for Identifying Seeded Defects in Gearboxes," Journal of Nondestructive Evaluation, **24**(1) pp. 11-28.

[17] Coy, J., Townsend, D., and Zaretsky, 1976, "Dynamic Capacity and Surface Fatigue Life for Spur and Helical Gears," ASME Journal of Lubrication, **98**(2) pp. 267–376.

[18] Boness, R. J., McBride, S. L., and Sobczyk, M., 1990, "Wear Studies using Acoustic Emission Techniques," Tribology International, **23**(5) pp. 291.

[19] Boness, R. J., and McBride, S. L., 1991, "Adhesive and Abrasive Wear Studies using Acoustic Emission Techniques," Wear, **149**(1-2) pp. 41-53.

[20] Yesilyurt, I., Gu, F., and Ball, A. D., 2003, "Gear Tooth Stiffness Reduction Measurement using Modal Analysis and its use in Wear Fault Severity Assessment of Spur Gears," NDT and E International, **36**(5) pp. 357-372.

[21] Saad Al-Dossary, R.I. Raja Hamzah, D. Mba, Observations of changes in acoustic emission waveform for varying seeded defect sizes in a rolling element bearing**, Journal of Applied Acoustics, Oct 2007. Accepted in press**

APPENDIX

Table A1 AE r.m.s and standard deviation (STD) values associated with each defect at different conditions

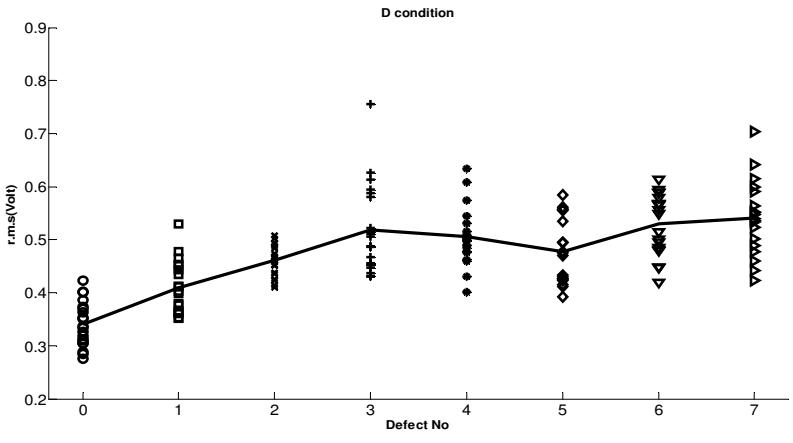

Figure A12 AE r.m.s level associated with defect condition 'D'

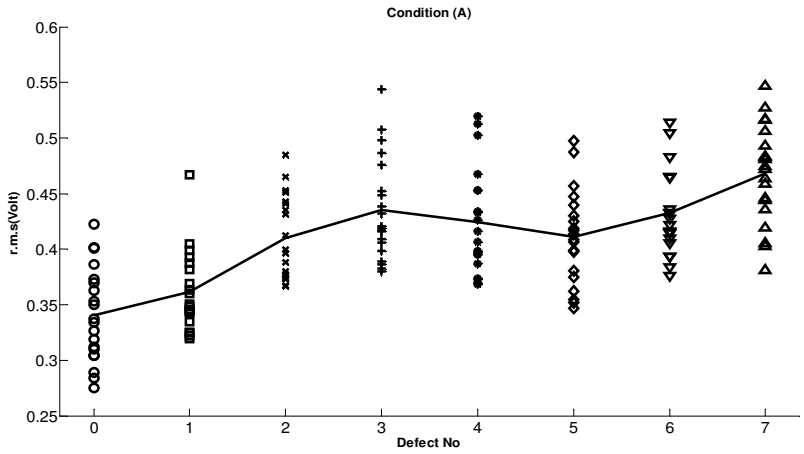

Figure A13 AE r.m.s level associated with defect condition 'A'

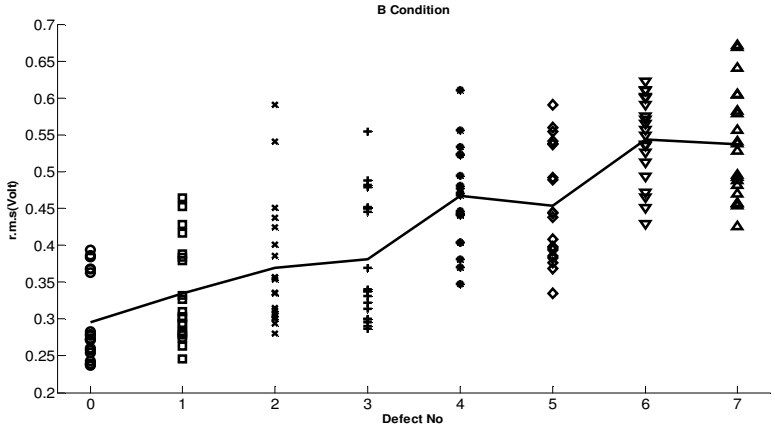

Figure A14 AE r.m.s level associated with defect condition 'B'

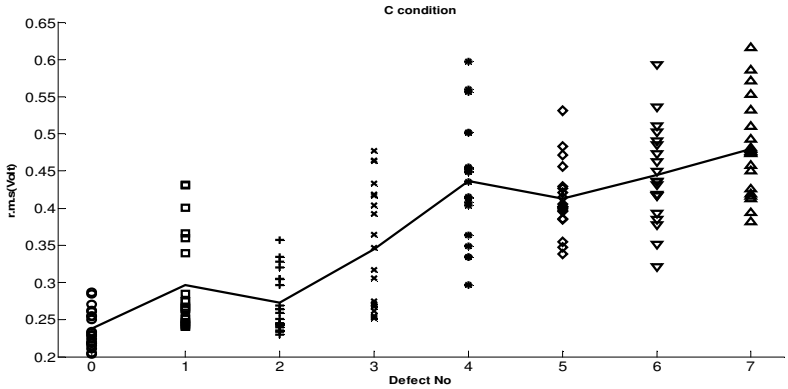

Figure A15 AE r.m.s level associated with defect condition 'C'